Materials and Design 136 (2017) 165–173

Contents lists available at ScienceDirect

Materials and Design

journal homepage: www.elsevier.com/locate/matdes

# Phase controlled synthesis of $CuSbS_2$ nanostructures: Effect of reaction conditions on phase purity and morphology

Mou Pal [a,*], Y. Torres Luna [b], R. Silva González [a], N.R. Mathews [c], F. Paraguay-Delgado [d], U. Pal [a]

[a] Instituto de Física, BUAP, Av. San Claudio y Blvd. 18 Sur Col. San Manuel, Ciudad Universitaria, C.P. 72570 Puebla, Mexico
[b] Faculty of Electronics, BUAP, Ciudad Universitaria, C.P. 72592 Puebla, Mexico
[c] Instituto de Energías Renovables, Universidad Nacional Autónoma de México, Temixco, Morelos 62580, Mexico
[d] Departamento de Materiales Nanoestructurados, Centro de Investigación en Materiales Avanzados (CIMAV), Chihuahua, Mexico

## HIGHLIGHTS

- Phase pure $CuSbS_2$ nanocrystals were syntheiszed by solvothermal method.
- Ethylenediamine (En), water and En-water mixture were used as reaction media.
- Use of binary solvent improves the crystallinity and changes drastically the shape and size of the $CuSbS_2$ nanostructures.
- The optical behavior and high yield of the product suggests the suitability of this material as solar absorber.

## GRAPHICAL ABSTRACT

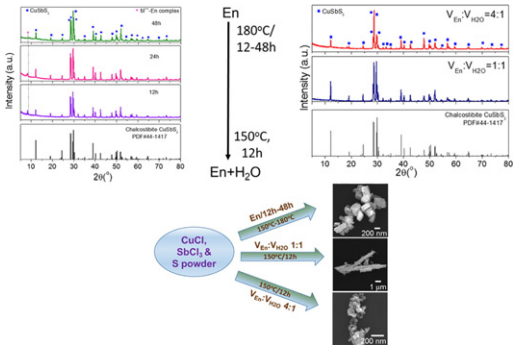


## ARTICLE INFO

*Article history:*
Received 29 March 2017
Received in revised form 3 September 2017
Accepted 26 September 2017
Available online 28 September 2017

*Keywords:*
$CuSbS_2$ nanostructures
Solvothermal synthesis
Binary solvent
Growth mechanism
Raman analysis

## ABSTRACT

Development of photovoltaic materials made of earth-abundant nontoxic elements is one of the primary goals of current energy research to meet the increasing demand of electrical energy worldwide. In this context, $CuSbS_2$ is proposed as an alternative absorber material for thin film solar cells due to its appropriate optical band gap, high absorption coefficient, and attractive power conversion efficiency (23%, theoretical). Here we report a surfactant-free solvothermal method using a mixed solvent constituting ethylenediamine (En) and deionized water for the synthesis of $CuSbS_2$ nanocrystals of different morphologies. The nature of solvent, reaction time and temperature of solvothermal treatment were found to have significant impacts on the shape and structural phase of $CuSbS_2$ nanostructures. Structural, optical and morphological properties of the nanostructures were thoroughly characterized using different techniques such as X-ray diffraction, Raman scattering, scanning electron microscopy, transmission electron microscopy, energy dispersive spectroscopy, X-ray photoelectron spectroscopy, and UV–Vis absorption spectroscopy. Effect of solvothermal conditions on the formation of stoichiometric, phase pure $CuSbS_2$ have been discussed.



## 1. Introduction

Research on the development of photovoltaic materials has been increased greatly in the current decade due to the shortage of fossil fuels that are the conventional resources to produce energy. Also the global

* Corresponding author.
*E-mail address:* mou@ifuap.buap.mx (M. Pal).

https://doi.org/10.1016/j.matdes.2017.09.059
0264-1275/

warming associated with the greenhouse gases released during the combustion of fossil fuels has forced the scientific community to search for alternative sustainable resources. In this context, thin film photovoltaics are considered as economically viable and practical solution to the world energy demand.

Thin film solar cell technology is currently dominated by cadmium telluride (CdTe) and copper indium gallium sulfide (CIGS), which serve as light absorbing materials due to their high absorption coefficient and adequate optoelectronic properties [1]. A remarkable power conversion efficiency beyond 20% has been reported for CdTe and CIGS based photovoltaic devices [2]. However, the toxicity concern associated with Cd and the limited abundance of the elements such as Te, Ga and In are the major restrictions for utilizing CdTe and CIGS based photovoltaic cells for massive terawatt scale energy production [3]. These restrictions prompted intensive research for the development of alternative photovoltaic materials consisting of earth abundant, low cost and non-toxic elements. Among such materials, SnS, $FeS_2$, $Cu_2S$, $Cu_2O$, $Cu_2ZnSn(S/Se)_4$ and $CuSbS_2$ have the prospect of showing high power conversion efficiency when incorporated as absorber layer in heterounion p-n junction photovoltaic devices [4–10]. While significant progress has been achieved on the development of solar cells based on $Cu_2ZnSn(S/Se)_4$, CdTe and CIGS, little attention has been paid to Cu-Sb-S systems as absorber materials. The potential of $CuSbS_2$ electrode in photovoltaic technology has been demonstrated by achieving 5%–15% of incident photon-to-current efficiency (IPCE) in the visible spectral region [11]. Copper antimony sulfides exist in four distinct phases such as chalcostibite ($CuSbS_2$), tetrahedrite ($Cu_{12}Sb_4S_{13}$), skinnerite ($Cu_3SbS_3$) and famatinite ($Cu_3SbS_4$) [12]. All of these phases have strong absorption coefficient ($\alpha > 10^5\ cm^{-1}$), p-type conductivity, and band gaps in the range of 1.1–1.8 eV [13,14]. In particular, $CuSbS_2$ has drawn special attention due to its suitable band gap in the range of 1.38–1.59 eV, followed by $Cu_{12}Sb_4S_{13}$ (1.6–1.7 eV) [15,16].

Since the last decade, synthesis of photovoltaic materials in the form of nanoparticles is of great interest. This approach is not only beneficial to prepare ink for the development of thin film solar cells in a cost-effective way, but also provides the opportunity to tune the optical properties of the material in nanometric regime. A number of chemical methods have been developed for the synthesis of different metal chalcogenides such as $Cu_2ZnSnS_4$, $Cu_2SnS_3$, $CuInGaSe_2$, $FeS_2$, SnS, $Cu_2O$, etc. in the form of nanocrystals [17–22]. However, only a few reports can be found in the literature on the synthesis of phase-pure $CuSbS_2$ nanocrystals with controlled size and morphology. Among them, the most common approach for the synthesis of copper antimony sulfide nanocrystals with different compositions is the hot injection method [12,23–25]. Beside this technique, Xu et al. reported the formation of Cu-Sb sulfide nanocrystals by thermal decomposition of diethyldithiocarbamate trihydrate complex of copper and antimony [26]. Yang et al. have fabricated $CuSbS_2$ films by spin coating of a hydrazine based stock solution of Cu, Sb and sulfur precursors, followed by thermal annealing [1]. An et al. reported a surfactant assisted hydrothermal method for the synthesis of $CuSbS_2$ nanorods [27]. Nevertheless, a simple, straightforward and surfactant-free synthetic protocol without employing any toxic or costly reactive is truly needed for the large scale production of photovoltaic nanocrystals. In particular, the use of long chain surfactants is not recommended in nanoparticle-based thin film approach as the surfactant can leave residual carbon impurities during thermal processing, which can significantly reduce device performance.

In this paper, we report the synthesis of phase pure chalcostibite $CuSbS_2$ nanocrystals through surfactant-free solvothermal process, which can be utilized to fabricate highly absorbing films for the fabrication of photovoltaic devices. Effect of synthesis parameters such as reaction time, temperature and the nature of solvent on the morphology, size, and crystalline phase of copper antimony sulfide nanocrystals have been studied. While chalcostibite phase could not be obtained in pure water under present solvothermal conditions, highly crystalline $CuSbS_2$ was formed in ethylenediamine (En) accompanied by a trace amount of stibnite $Sb_2S_3$. However, the main inconvenience of $CuSbS_2$ preparation in pure En was the formation of a well-crystalline metal ion-En complex. Interestingly, the use of a binary solvent made of En and water not only produced pure chalcostibite $CuSbS_2$ under mild solvothermal conditions, but also inhibited the formation of the metal ion-En complex. The variation of $V_{En}$:$V_{H2O}$ ratio was found to have a pronounced effect on the shape of the resulting product. The structural, optical, and compositional properties were thoroughly investigated using different characterization tools. The high yield and employment of mild reaction conditions have added good prospects for large scale production of chalcostibite $CuSbS_2$ nanocrystals.

## 2. Experimental

### 2.1. Materials

Copper (I) chloride dihydrate ($CuCl \cdot 2H_2O$, Sigma-Aldrich), antimony (III) chloride ($SbCl_3$, Sigma Aldrich), sulfur powder (Sigma-Aldrich) and ethylenediamine ($NH_2CH_2CH_2NH_2$, J.T. Baker) were used as received. Deionized water (DI, $\rho > 18.2\ M\Omega \cdot cm$) used throughout the experiment was produced by a Milli-Q water purification system.

### 2.2. Synthesis

In a typical experimental procedure, 5 mM of CuCl and 5 mM of $SbCl_3$ were dissolved either in 50 mL of ethylenediamine (En) or in a certain amount of deionized water. In the case of En as solvent, 12.5 mM of sulfur powder was added to the metal ion containing En solution and continued stirring for another 25 min, obtaining a green viscous solution. For En-water binary solvent, 12.5 mM sulfur powder was separately dissolved in a certain volume of En and added into the metal ion containing aqueous solution, followed by thorough mixing under constant stirring. Keeping the total volume of the binary solvent fixed (50 mL), the volumetric ratio of En and water was varied either $V_{En}$:$V_{H2O}$ = 4:1 or $V_{En}$:$V_{H2O}$ = 1:1. Finally, the resulting solution was transferred to a Teflon-lined stainless steel autoclave which was sealed and maintained either at 150 or 180 °C for a certain incubation period. When the autoclave reached to the room temperature, the black precipitate was centrifuged and washed with deionized water and ethanol several times to remove all the unreacted ions. The sample was dried overnight at room temperature before characterization. The ethylenediamine based precursor solution was subjected to several different solvothermal conditions: 150 °C for 12 h; 150 °C for 24 h; and 180 °C for 12, 24 and 48 h, whereas the precursor mixture in binary solvent was subjected uniquely to 150 °C for 12 h. In each batch of synthesis, we obtained approximately 1 g of $CuSbS_2$ powder sample. A schematic representation of the experimental procedure utilized for synthesizing the $CuSbS_2$ nanostructures is presented in Fig. 1.

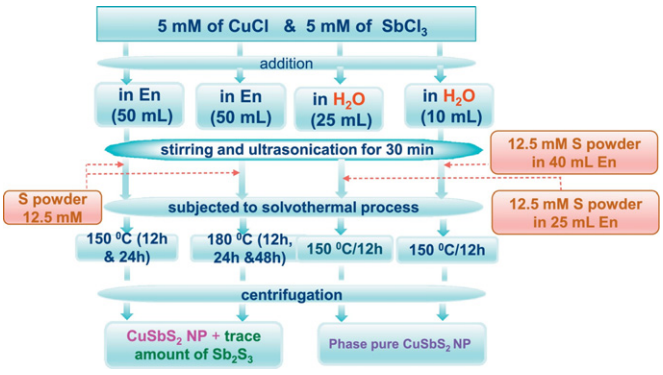


**Fig. 1.** Flow diagram showing the multiple steps and conditions utilized for the synthesis of $CuSbS_2$ nanostructures.

### 2.3. Characterization

The crystallinity and structural phase analysis of the samples were performed utilizing CuKα radiation (λ = 1.5406 Å) radiation on a Bruker D8 DISCOVER X-ray diffractometer operating at 25 keV and 25 mA. Room temperature Raman spectra of the samples were recorded on a Lab RAM micoRaman spectrometer (Horiba Jobin Yvon HR800) using 632.8 nm emission of a He-Ne laser. A field emission scanning electron microscope (FE-SEM, JSM-7800F JEOL) attached with Oxford analytical system operating at 15 keV was utilized to analyze the morphology and elemental composition of the synthesized samples. To get further insight on the size, shape and fine structure of the $CuSbS_2$ nanocrystals, low and high resolution images were acquired on a JEOL JEM 200FS high-resolution transmission electron microscope (HRTEM) operating at 200 keV. Optical properties of the powder samples were evaluated on a Varian Cary UV–Vis spectrophotometer equipped with DRA-CA-30I diffuse reflectance accessory. The chemical states of the elements were determined from the X-ray photoelectron spectra recorded using a K-Alpha (Thermo Scientific) X-ray photoelectron spectrometer. Binding energies of each element were calibrated using C1s energy at 284.6 eV. The results of XPS analysis are discussed in the supporting information.

## 3. Results and discussion

### 3.1. XRD analysis

Fig. 2 presents the XRD patterns of $CuSbS_2$ samples obtained using ethylenediamine as solvent under different solvothermal conditions. In this study, we varied both the reaction time and temperature to optimize the process for producing highly crystalline, phase pure chalcostibite. For all the three samples, the positions and relative intensities of the diffraction peaks are in well accordance with those of the orthorhombic crystal structure of chalcostibite $CuSbS_2$ (JCPDS # 44-1417). In the case of the samples obtained at 150 °C, a minor $Sb_2S_3$ phase (Fig. 2a & b; marked with asterisk) was detected, even though the reaction time was increased from 12 h to 24 h. However, the intensity of this secondary phase is much lower for longer reaction period (Fig. 1b). With the increase of solvothermal temperature from 150 to 180 °C, we could eliminate the $Sb_2S_3$ phase even for a shorter incubation period of 12 h (Fig. 2c). It is important to note that although the orthorhombic phase of $CuSbS_2$ could be achieved through solvothermal treatment of the precursors at temperature as low as 150 °C for an incubation period of 12 or 24 h, their XRD spectra reveal an intense diffraction peak at 2θ ~9.5°, which does not coincide with any of the possible secondary phases of Cu-Sb-S system. The same peak appeared with much lower intensity on increasing the temperature to 180 °C (Fig. 2c).

In order to investigate if a prolonged solvothermal treatment helps to avoid the formation of this unidentified phase, two more samples were prepared at 180 °C for 24 and 48 h and analyzed by XRD (Fig. 3). The results indicate that a longer duration of solvothermal treatment at 180 °C helps to dissociate this impurity phase.

To verify the effect of solvent on the formation of this unidentified phase, we prepared the nanostructures in a binary solvent containing water and En in different volume ratios. For that, CuCl and $SbCl_3$ were dissolved in water while sulfur powder in ethylenediamine. The solvothermal treatment was performed at 150 °C for 12 h. The as-grown nanostructures were analyzed by XRD and displayed in Fig. 4. All of the peaks appeared in the diffraction pattern match well with the orthorhombic phase of chalcostibite $CuSbS_2$, according to the standard PDF# 44-1417. The PDF card for tetrahedrite $Cu_{12}Sb_4S_{13}$ phase (PDF# 24-1318) has also been included to compare the XRD patterns as this phase was detected in trace amount in the Raman spectra. Interestingly, the diffraction peak belonging to the unidentified phase did not appear for these samples, even though they were prepared under mild solvothermal conditions of 150 °C for 12 h. The observation strongly suggests that the peak appearing at lower diffraction angle (2θ <10°) is due to the formation of a chelated complex of En and transition metal ions ($M^{n+}$), which does not form when the metal salts are dissolved in water. The XRD results suggest that this metalorganic complex ($M^{n+}$-En) is stable up to 150 °C, and at around 180 °C it starts to lose its stability (Fig. 2). The assumption behind the formation of this type of metal-En complex is quite valid because of the bidentate chelating action of ethylenediamine with transition metal ions ($Cu^{+}$ and $Sb^{3+}$) present in the reaction medium.

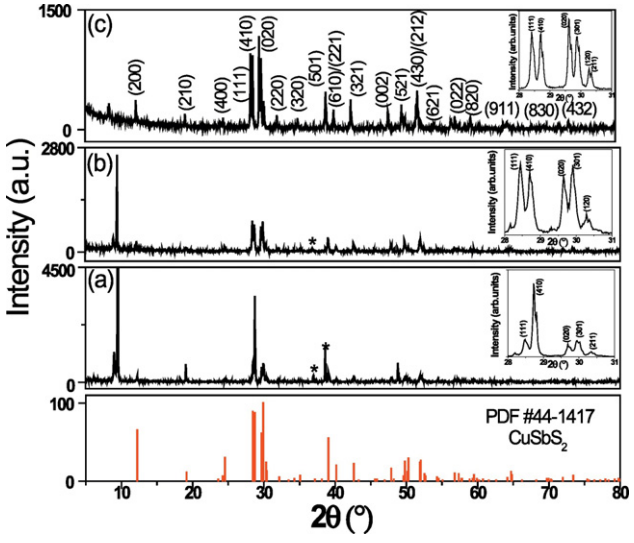


**Fig. 2.** XRD patterns of the $CuSbS_2$ samples synthesized solvothermally using ethylenediamine as solvent at: (a) 150 °C/12 h, (b) 150 °C/24 h and (c) 180 °C/12 h. Insets of each XRD pattern show the part of the corresponding diffractogram in the 28–31° 2θ range (surrounded by dotted rectangles) in order to appreciate clearly the closely spaced characteristic reflections of the samples. * corresponds to $Sb_2S_3$ stibnite phase. In the case of the XRD patterns 1(a)–(c), the peak surrounded by red ovals (at 2θ <10°) do not belong to any secondary phase of Cu-Sb-S system. The red vertical lines indicate the position and relative intensity of the diffraction peaks of pure chalcostibite phase (JCPDS # 44-1417). (For interpretation of the references to colour in this figure legend, the reader is referred to the web version of this article.)

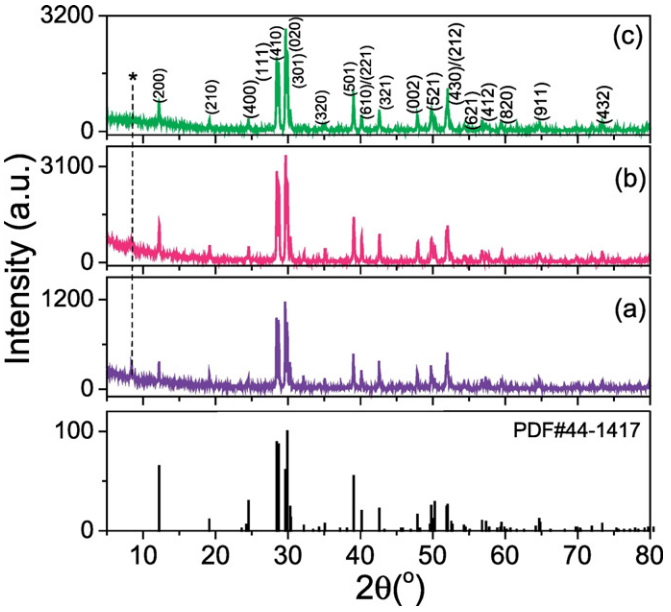


**Fig. 3.** XRD patterns of $CuSbS_2$ samples synthesized by solvothermal treatment of the precursors at 180 °C for different incubation periods: (a) 12 h, (b) 24 h, and (c) 48 h.

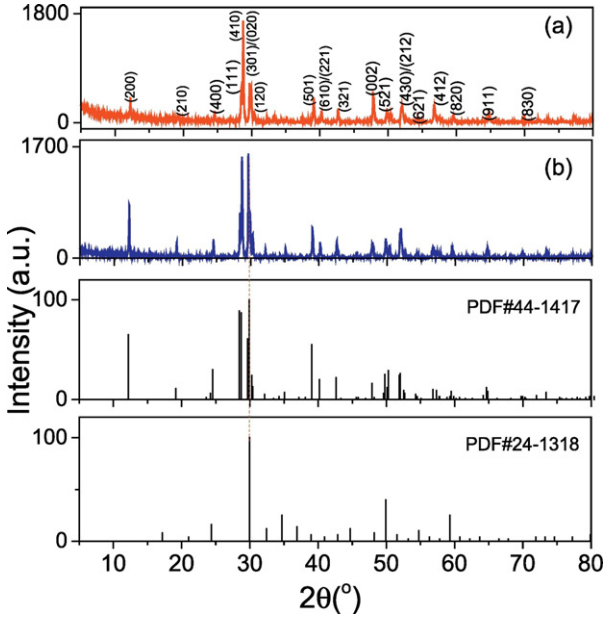


**Fig. 4.** XRD pattern of $CuSbS_2$ samples obtained by solvothermal treatment at 150 °C and 12 h, for $V_{En}$:$V_{H2O}$: (a) 4:1 and (b) 1:1.

The formation of $CuSbS_2$ in presence of En under the present solvothermal conditions can be described in the following steps: (1) the coordination of ethylenediamine with metal ions ($M^{n+} = Cu^+$ and $Sb^{3+}$) to form a $[M^{n+}(En)_m]$ complex, where m = coordination number of metal ions; (2) reduction of elemental sulfur to $S^{2-}$ by En; (3) the reaction between $[M^{n+}(En)_m]$ and $S^{2-}$ to form an intermediate $MS_2(En)_m$ structure; and (4) elimination of En molecule from the $MS_2(En)_m$ under high pressure and temperature to form the ternary metal sulfide. A general reaction scheme involved in the solvothermal process for producing $CuSbS_2$ nanostructures is shown below.

$$M^{n+}\left(Cu^{+}/Sb^{3+}\right) + m\,En \rightarrow [M^{n+}(En)_m] \quad (1)$$

$$S + 2e \xrightarrow{En} S^{2-} \quad (2)$$

$$[Mn + (En)_m] + 2S^{2-} \rightarrow MS_2(En)_m \quad (3)$$

$$MS_2(En)_m \rightarrow MS_2 + m\,En \quad (4)$$

where $M^{n+} = Cu^+ / Sb^{3+}$.

A detailed description about the multifunctional role of En as chelating ligand, reducing agent and excellent S-solvation can be found in our previous works [17,28]. It is important to mention that we could not obtain ternary $CuSbS_2$ phase in pure water even after several trials by careful tuning of temperature, time and precursor concentration. In all the cases, either stibnite $Sb_2S_3$ or a mixture of binary phases like $Sb_2S_3$ and $Cu_9S_8$ were obtained as main products (Supporting information). In the case of pure water as solvent, we used thioacetamide instead of sulfur powder as S-source due to the absolute insolubility of sulfur in water. We assume that the autogenous pressure created under the applied hydrothermal conditions was probably not sufficient to produce ternary Cu-Sb-S phases.

### 3.2. Raman study

The crystallinity and structural phase of the powder samples were further verified through Raman scattering study. Fig. 5 displays the Raman spectra of $CuSbS_2$ samples obtained under different solvothermal conditions. As can be seen, they are pretty similar to each other, irrespective of the reaction temperature, time and type of solvent. In all the cases, the Raman spectra are dominated by a dispersion peak at around 333 $cm^{-1}$, along with other vibrational modes appearing around 162 and 251 $cm^{-1}$, which belong to the characteristic phononic vibrations of chalcostibite $CuSbS_2$ phase [15,29]. A further increase in temperature from 150 to 180 °C resulted in the evolution of a minor peak at 358 $cm^{-1}$ along with the characteristic peaks of chalcostibite phase, which disappears on increasing the incubation period from 12 h to 24 or 48 h (Fig. 5b). This peak can be associated with the tetrahedrite $Cu_{12}Sb_4S_{13}$ phase, which was reported to form at relatively higher temperature (~180 °C) [12,15]. In the case of binary solvent, in addition to the characteristic Raman peak of chalcostibite at 334 $cm^{-1}$, a low intensity peak was found to appear at around 316 $cm^{-1}$ corresponding to $A_g$ symmetry of $CuSbS_2$ phase [30,31]. According to Baker et al., the 316 $cm^{-1}$ peak should be of 30% of less intense compared to the major Raman peak of chalcostibite at 334 $cm^{-1}$ which is in good agreement with our results. Therefore, the structural

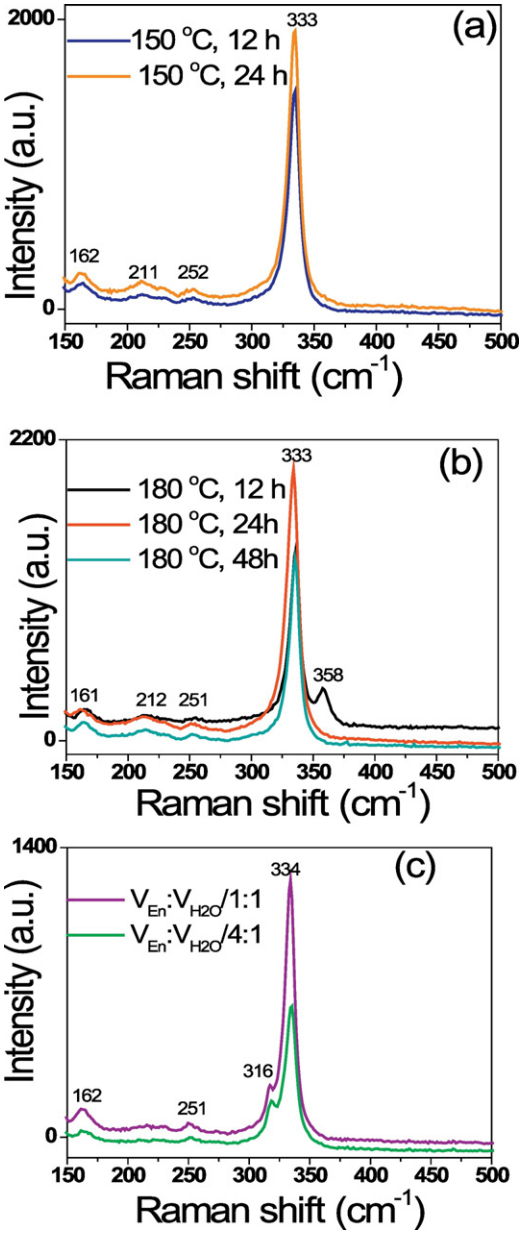


**Fig. 5.** Raman spectra of $CuSbS_2$ synthesized under different solvothermal conditions: (a) in ethylenediamine/150 °C/12 or 24 h, (b) in ethylenediamine/180 °C/12, 24 or 48 h, and (c) binary solvent with variable $V_{En}$:$V_{H2O}$/150 °C/12 h.

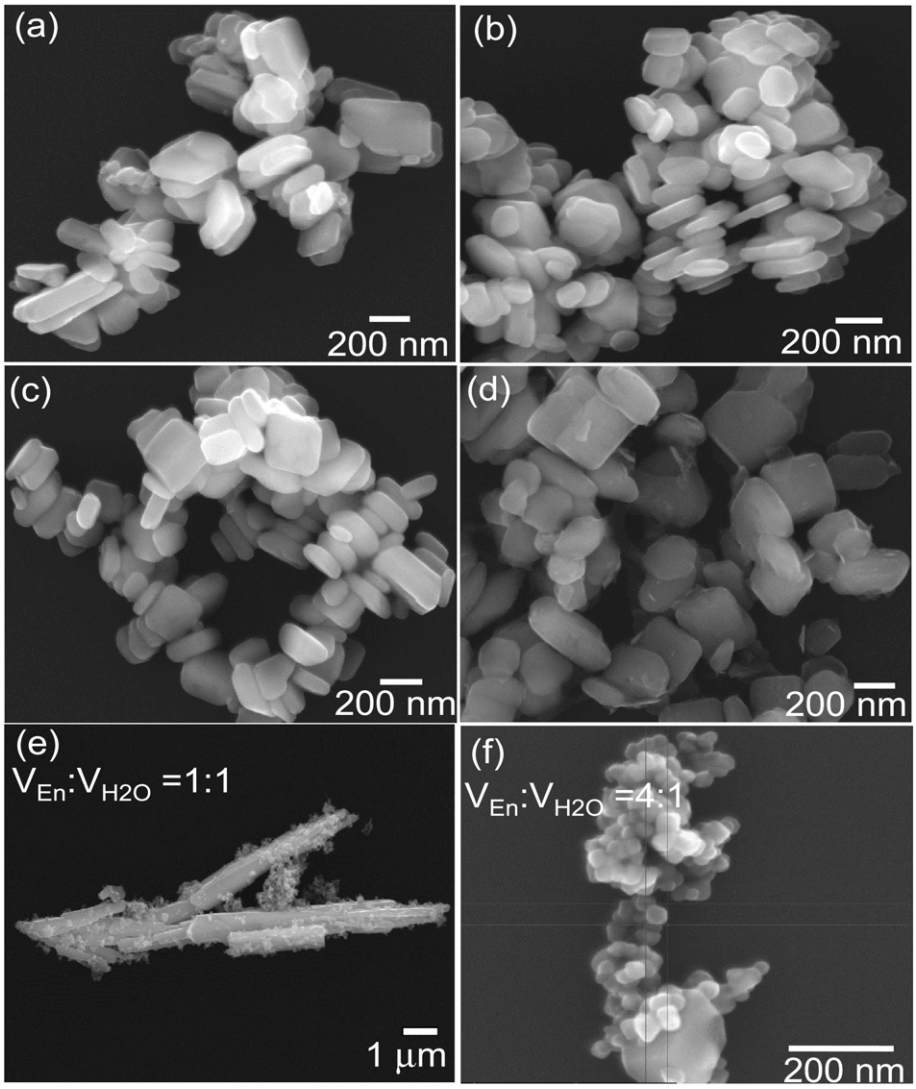


**Fig. 6.** Typical SEM images of the $CuSbS_2$ nanostructures grown under different solvothermal conditions: (a) En/150 °C/12 h, (b) En/150 °C/24 h, (c) En/180 °C/12 h, (d) En/180 °C/48 h, (e) En/150 °C/12 h/$V_{En}$:$V_{H2O}$ = 1:1 and (f) En/150 °C/12 h/$V_{En}$:$V_{H2O}$ = 4:1.

analysis based on Raman spectroscopy firmly supports the formation of phase pure chalcostibite in the binary solvent without the presence of metal complex or tetrahedrite $Cu_{12}Sb_4S_{13}$ phase.

### 3.3. SEM study

The morphology and size of the nanocrystals were analyzed in the first instance by a scanning electron microscope (SEM). Fig. 6 presents typical SEM images of $CuSbS_2$ nanostructures obtained under different synthesis conditions. In the case of solvothermal temperature of 150 °C and ethylenediamine as solvent (Fig. 6a and b), the brick-shaped morphology predominates with a slight variation in the average particle size depending on the incubation period. While particles with an average length of 300 nm ± 97 nm and width of 105 nm ± 45 nm were obtained for an incubation period of 12 h (Fig. 6a), nanostructures with a slightly smaller aspect ratio (216 nm ± 44 nm in length and 98 ± 25 nm of width) were formed for longer reaction time (Fig. 6b). Co-existence of a few cuboid, oval and irregular-shaped particles can also be observed in the micrographs. It is reported in the literature that ethylenediamine forms an intermediate of $MS_2$-En complex-layered structure during the solvothermal growth of metal chalcogenides [32]. We assume that at longer reaction time, the observed shrinkage in length and width is due to the elimination of En-complexes attached in between the layered structures.

When the solvothermal temperature was increased to 180 °C for 12 h in the same En solvent, the brick shaped morphology was still

**Table 1**
Morphological and structural characteristics of $CuSbS_2$ nanocrystals obtained under different solvothermal conditions.

| Growth conditions | Obtained structural phases | Morphology | Aspect ratio |
|---|---|---|---|
| En/150 °C/12 h | Chalcostibite, $Sb_2S_3$, metal-complex | Nanobricks | 2.85 |
| En/150 °C/24 h | Chalcostibite, $Sb_2S_3$, metal-complex | Nanobricks | 2.20 |
| En/180 °C/12 h | Chalcostibite, metal-complex | Nanobricks | 3.0 |
| En/180 °C/48 h | Chalcostibite | Agglomerated nanobricks | – |
| En/$H_2O$/150 °C/12 h ($V_{En}$:$V_{H2O}$ = 1:1) | Chalcostibite | Microrods and nanoparticles | 20 |
| En/$H_2O$/150 °C/12 h ($V_{En}$:$V_{H2O}$ = 4:1) | Chalcostibite | Spheres with faceted faces | – |

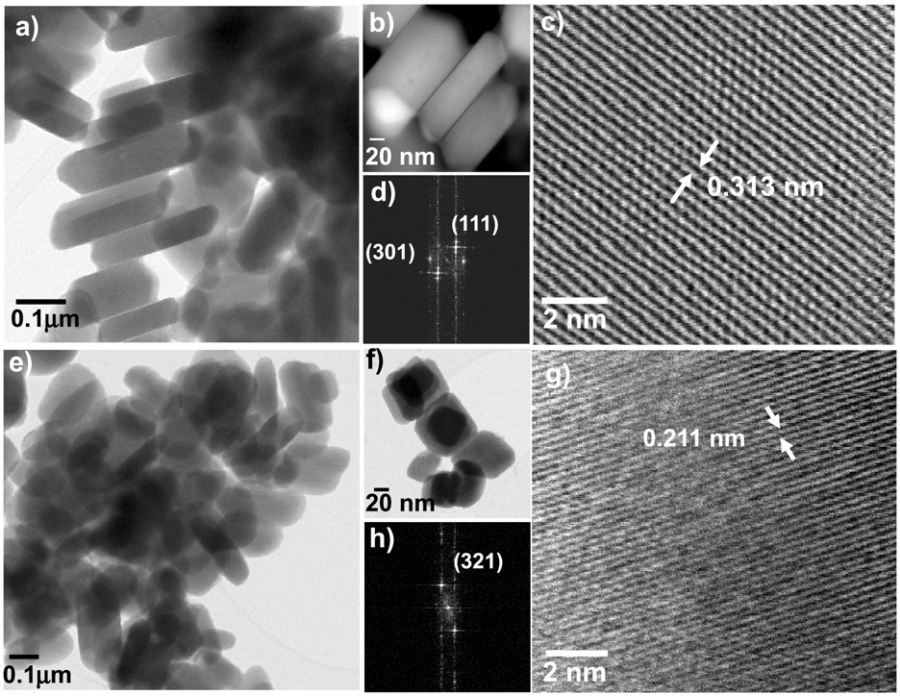


**Fig. 7.** Typical TEM images of $CuSbS_2$ nanostructures obtained in ethylenediamine under different solvothermal conditions. Upper and lower panels correspond to samples prepared at 150 °C/24 h and 180 °C/24 h respectively: (a–b) and (e–f) are TEM images, (c & g) are the HRTEM images and (d & h) are the fast Fourier transform patterns of the corresponding HRTEM images.

preserved (Fig. 6c). However, on increasing the processing time up to 48 h, they tend to agglomerate, resulting in the formation of elongated and cuboid-shaped nanoplates (Fig. 6d). The length and width of $CuSbS_2$ nanocrystals obtained by solvothermal method for 12 h varied in between 250–300 nm and 75–100 nm, respectively. In all the cases, the brick-shape or nanoplate morphology is governed by the layered structure of $CuSbS_2$ semiconductor [12].

On switching to a binary solvent containing water and En under mild solvothermal condition (150 °C/12 h), the morphology of the $CuSbS_2$ particles has been drastically changed. While $V_{H2O}$:$V_{En}$ = 1:1 leads to a mixed morphology containing microrods (length: 2–3 μm and width: 150–170 nm) and nanoparticles (diameter: 90–100 nm) (Fig. 6e), a lower water content in the binary solvent produces quasi-spherical faceted nanocrystals with diameter in the range of 40–

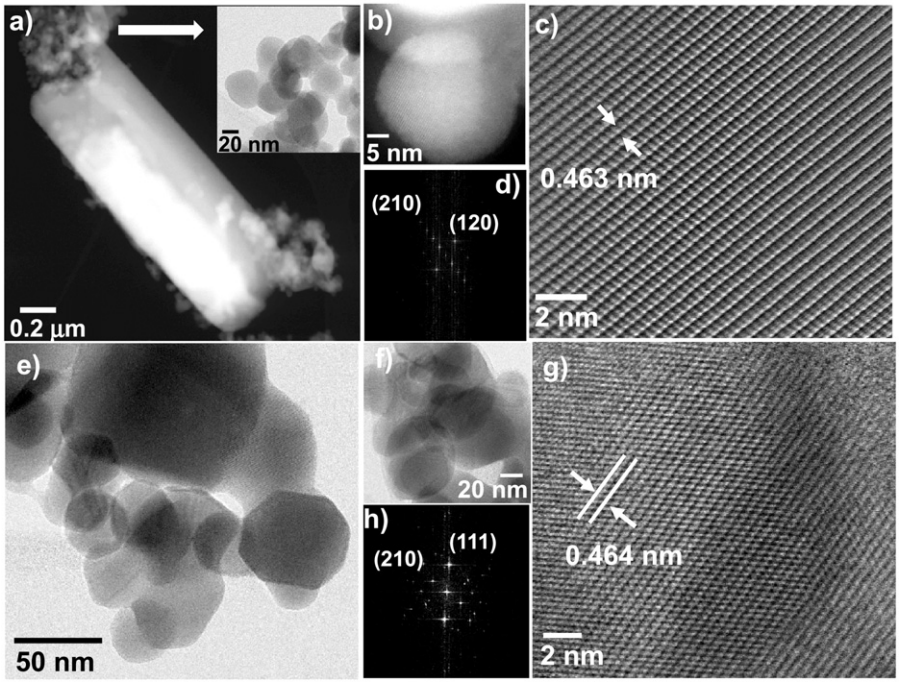


**Fig. 8.** Representative TEM micrographs of $CuSbS_2$ nanostructures obtained in a binary solvent at 150 °C for 12 h. The upper panel represents the sample grown at $V_{En}$:$V_{H2O}$ = 1:1 while the lower panel corresponds to the sample obtained with $V_{En}$:$V_{H2O}$ = 4:1.

**Table 2**
EDS estimated elemental composition of the $CuSbS_2$ (CAS) nanocrystals obtained at different solvothermal conditions. CAS-A: En/150 °C/24 h, CAS-B: En/180 °C/24 h, CAS-C: $V_{En}$:$V_{H2O}$ 1:1/150 °C/12 h, and CAS-D: $V_{En}$:$V_{H2O}$ 4:1/150 °C/12 h.

| Atomic ratio | CAS-A | CAS-B | CAS-C | CAS-D |
|---|---|---|---|---|
| Cu/Sb/S | 28.2/23.62/48.18 | 31.06/22.32/46.62 | 30/22.64/47.36 | 26.72/25.27/48.0 |

65 nm (Fig. 6f) along with some aggregated clusters as big as 100–200 nm. The formation of long sheet or plate-like structures with ~5 μm in length and ~500 nm in width (Fig. 6e) might be due to the aggregation of individual microrods. Table 1 summarizes the structural and morphological characteristics of different $CuSbS_2$ nanocrystals determined by XRD analysis and SEM images study.

It is worth noting that the type of solvent has a significant impact on the preferential growth direction of $CuSbS_2$. The formation of elongated structures requires high concentrations of $CuSbS_2$ nuclei (i.e., monomer) in the initial growth stage. As the synthesis of $CuSbS_2$ in pure En proceeds through the formation of coordination complex, the stability of this complex greatly influences the concentration of $CuSbS_2$ nuclei in the bulk solution. More stable is the complex, less nuclei are present in the solution; thereby favoring the isotropic growth. It has been known that the stability of the metal complex is directly proportional to the dielectric constant value of the solvent [33]. Therefore, in a solvent with low dielectric constant such as ethylenediamine ($\varepsilon = 13.82$), the metal-En complex is not stable resulting in a high monomer concentration which satisfies the condition for anisotropic growth of $CuSbS_2$ nanostructures. This explanation clearly describes the formation of brick shape $CuSbS_2$ particles in pure En as can be observed in Fig. 6a–d. When a binary solvent such as water-En mixture was used, the net dielectric constant is higher compared to pure En, as water has a high dielectric constant value of 80.1 [34]. The presence of a solvent with higher dielectric constant tends to dissolve the $CuSbS_2$ nuclei into their respective ions. Since the monomer concentration is low in the reaction medium, the formation of brick- like structures can be ruled out. Under such condition, the growth of spherical particles takes place through the equilibrium crystal growth [35]. In our experiment, when both En and water were present in same volume ratio ($V_{En}$:$V_{H2O}$ = 1:1), the occurrence of anisotropic as well as isotropic growth of nanocrystals were observed (Fig. 6e). On the other hand, by reducing the water ratio in binary solvent ($V_{En}$:$V_{H2O}$ = 4:1), the net dielectric constant was tuned to a value slightly higher than that of En, which instead of favoring elongated brick-shaped particles, leads to the formation of faceted quasi-spherical particles (Fig. 6f).

### 3.4. TEM study

TEM micrographs of $CuSbS_2$ nanocrystals (NCs) obtained in pure ethylenediamine are shown in Fig. 7. The upper panel corresponds to the samples prepared at 150 °C while the lower panel is for the $CuSbS_2$ nanostructures obtained at 180 °C; in both cases the processing time was 24 h. The NCs obtained at 150 °C/24 h (Fig. 7a–b) show well-defined rod-like structures with pyramidal tips. The length of the shorter nanorods lies in between 150 and 165 nm and the longer structures possess a length close to 270 nm. The width of the rods in each case was in between 50 and 55 nm. Typical HRTEM image of the nanostructures presented in Fig. 7c revealed a lattice spacing of about 0.313 nm, which corresponds to the (111) plane of chalcostibite $CuSbS_2$ phase. The corresponding fast Fourier transform (FFT) revealed the reflections from (111) and (301) planes of $CuSbS_2$ (Fig. 7d). The NCs obtained by a solvothermal processing at 180 °C for 24 h revealed ellipsoidal to cuboid shapes (Fig. 7e–f). The shorter particles have an approximate length of 125–150 nm and a width of 55–60 nm while the larger nanostructures have a length close to 235 nm and width of 75–80 nm. Instead of pyramidal tips the particles have smooth edges. The lattice spacing measured directly from the HRTEM image (Fig. 7g) as well as the corresponding FFT (Fig. 7h) gives a value of 0.21 nm, which could be indexed to (321) plane of orthorhombic $CuSbS_2$.

Fig. 8 shows the TEM images of $CuSbS_2$ NCs obtained in the binary solvent at 150 °C for 12 h. The upper and lower panels correspond to the samples prepared in En/$H_2O$ with 1:1 and 4:1, volume ratio, respectively. In the case of $V_{En}$:$V_{H2O}$ 1:1, two type of morphologies appeared including rods and tiny nanoparticles (Fig. 8a). The microrods have an average diameter of 350 nm and lengths close to 2 μm. The inset of Fig. 8a shows a magnified image of tiny spherical nanoparticles. An individual spherical particle with diameter ~35 nm is shown in Fig. 8b. The HRTEM image in Fig. 8c shows the continuous and parallel lattice fringes with excellent contrast, suggesting the high crystallinity of the product. The distance between adjacent lattices measured directly on the HRTEM image gave a value of 0.463 nm, corresponding to (210) plane. The corresponding FFT pattern (Fig. 8d) shows bright spots corresponding to (210) and (120) crystal faces of orthorhombic $CuSbS_2$ (PDF card no. 44-1417).

By decreasing the water fraction in the binary solvent under otherwise same experimental conditions, spherical nanoparticles of diameters in the range of 40–65 nm were formed (Fig. 8e–f) along with some aggregated clusters as big as 100–200 nm. The HRTEM image in Fig. 8g revealed well-defined lattice planes with average spacing of 0.464 nm, which corresponds to the inter planer spacing (*d* value) of (210) planes. The corresponding FFT pattern, presented in Fig. 8h, matches well with the (210) and (111) crystal faces of chalcostibite $CuSbS_2$ (PDF card no. 44-1417).

### 3.5. EDS analysis

The elemental composition of the samples was estimated by analyzing their EDS spectra. To verify the compositional homogeneity of the nanostructures, EDS analyses were performed at seven different locations for each sample. Estimated multipoint average compositions of the prepared samples are summarized in Table 2. The composition of all the samples were slightly rich in copper and deficient in sulfur; however, the sample CAS-D (the sample prepared at 150 °C, 12 h in binary solvent with $V_{En}$:$V_{H2O}$ = 4:1) was the closet to ideal stoichiometry.

### 3.6. Optical properties

The information about the light absorbing capacity of a semiconducting material is highly significant for its specific application. $CuSbS_2$

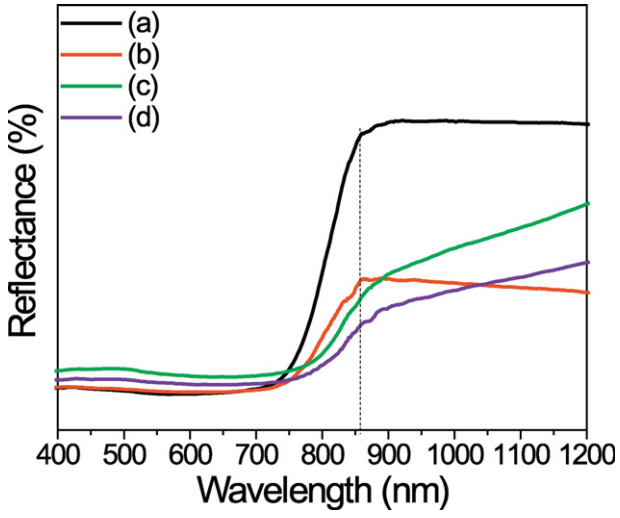


**Fig. 9.** Diffuse reflectance spectra of the $CuSbS_2$ nanostructures prepared at different solvothermal conditions: (a) En/150 °C/24 h, (b) En/180 °C/24 h, (c) $V_{En}$:$V_{H2O}$ = 1:1/150 °C/12 h, (d) $V_{En}$:$V_{H2O}$ = 4:1/150 °C/12.

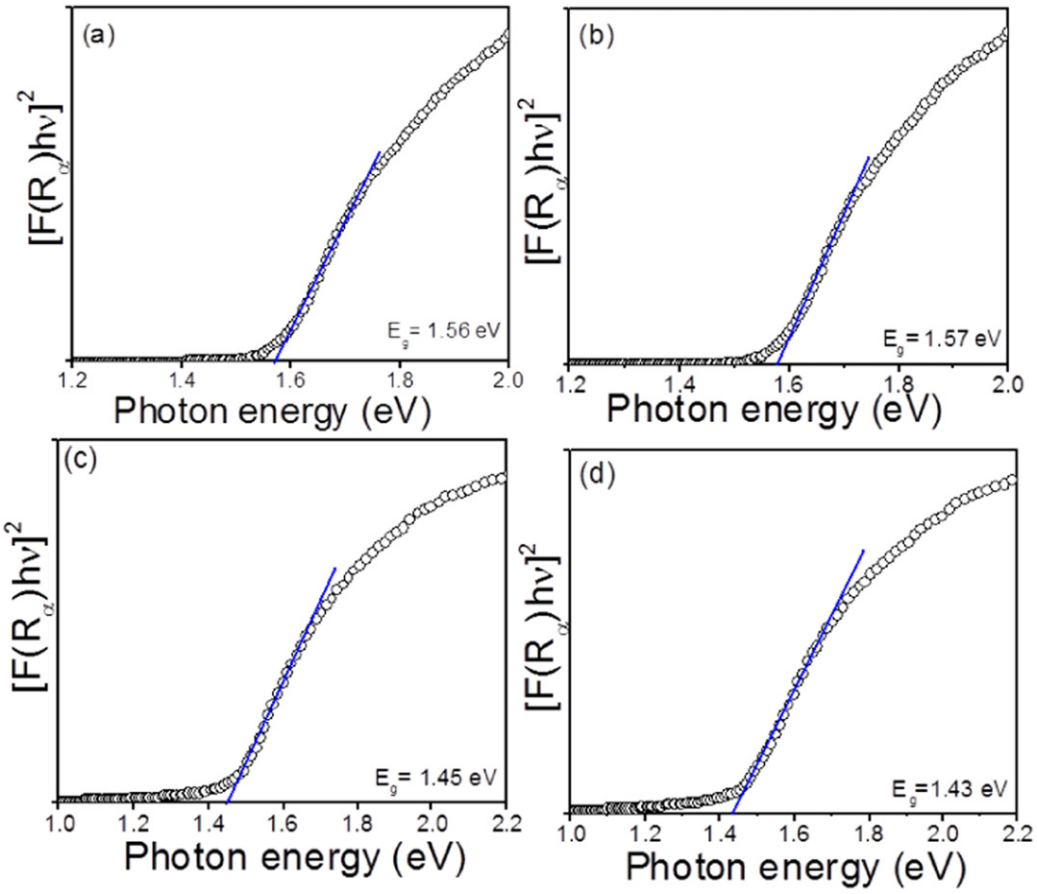


**Fig. 10.** Kubelka-Munk plots used to estimate the direct optical band gap values of $CuSbS_2$ nanostructures grown under different solvothermal conditions: (a) En/150 °C/24 h, (b) En/180 °C/24 h, (c) $V_{En}$:$V_{H2O}$ = 1:1/150 °C/12 h, (d) $V_{En}$:$V_{H2O}$ = 4:1/150 °C/12 h.

has been considered as an important photovoltaic material due to its tunable band gap and high light absorption capacity in ultraviolet and visible regions [36]. To evaluate the optical properties of our $CuSbS_2$ nanostructures, UV–vis spectroscopy was performed on the powder samples in diffuse reflectance mode. As can be seen in Fig. 9, all the samples exhibit a sharp reduction in reflectance at around 850 nm, implying their good light absorption capacity in the visible light spectrum.

By using the Kubelka-Munk formalism, the reflectance spectra of all the four powder samples were transformed into Kubelka-Munk coefficient, $F(R_\alpha)$, utilizing the relation [37]:

$$F(R_\alpha) = (1-R_\alpha)^2/2R_\alpha$$

where $R_\alpha$ is the reflectance of an infinitely thick sample with respect to a reference (Teflon) at each wavelength. The optical band gap values for all the four samples were determined by plotting $[F(R_\alpha)h\nu]^n$ versus $h\nu$ ($h$ is Plank's constant, $\nu$ = frequency; n = 1/2 for direct transition) and extrapolating the linear portion of the plot to the photon energy axis (Fig. 10).

The results show that the $CuSbS_2$ nanocrystals possess direct band gap ($E_g$) varying in between 1.43 eV to 1.57 eV, depending on the conditions of solvothermal processing. The band gap values and absorption behaviors of the samples are consistent with previous reports [16, 23–25]. The appropriate band gaps and other structural features make our $CuSbS_2$ nanocrystals interesting for photovoltaic applications.

## 4. Conclusions

Well crystalline, near stoichiometric, shape defined $CuSbS_2$ nanostructures of pure orthorhombic phase could be synthesized by solvothermal process by optimizing reaction conditions and solvent composition. While the use of pure En as solvent produces chalcostibite $CuSbS_2$ accompanied by a trace amount of stibnite $Sb_2S_3$, the use of binary solvent leads to the formation of pure chalcostibite phase (without the trace of any other phase) under similar reaction conditions. The disadvantage of using pure En as solvent is the formation of metal-En complex, which does not dissociate below 180 °C. A trace amount of tetrahedrite phase was formed in the samples prepared in binary solvent and a possible explanation has been put forward to understand its formation. The volume fraction of water in the binary mixture solvent also controls the shape and size of $CuSbS_2$ nanostructures. A growth mechanism has been proposed to explain the formation of $CuSbS_2$ with different morphologies, while switching the solvent from ethylenediamine to binary one. The method proposed in this work might be useful for the fabrication of other ternary sulfide nanostructures with controlled size, morphology and composition at large scale. The development of $CuSbS_2$ films using the nanoparticle-based paste with subsequent heat treatment and evaluation of their structural and photovoltaic properties are underway.

## Acknowledgements

The authors are sincerely thankful to CUVyTT, BUAP for XRD analysis. Authors wish to acknowledge the projects PRODEP-SEP, Mexico (Grant # DSA/103.5/15/7449, PROFOCIE-2016) and VIEP-BUAP (Grant # VIEP/EXC-2017), PAPIIT IN 107815 for the financial support received for the development of nanomateriales. This work has collateral application in the project Conjunta de Movilidad 2015 CONACyT-DST #266406. The authors are sincerely thankful to Dr. B. Krishnan of Universidad Autónoma de Nuevo León, Mexico for XPS measurements.

## Appendix A. Supplementary data

Supplementary data to this article can be found online at https://doi.org/10.1016/j.matdes.2017.09.059.

## References


[1] B. Yang, L. Wang, J. Han, Y. Zhou, H. Song, S. Chen, Jie Zhong, Lu Lv, D. Niu, J. Tang, Chem. Mater. 26 (2014) 3135–3143.
[2] M.A. Green, K. Emery, Y. Hishikawa, W. Warta, E.D. Dunlop, D.H. Levi, A.W.Y. Ho-Baillie, Prog. Photovolt. Res. Appl. 25 (2017) (2017) 3–13.
[3] D.B. Mitzi, O. Gunawan, T.K. Todorov, K. Wang, S. Guha, Sol. Energy Mater. Sol. Cells 95 (2011) 1421–1436.
[4] T.K. Todorov, J. Tang, S. Bag, O. Gunawan, T. Gokmen, Y. Zhu, D.B. Mitzi, Adv. Energy Mater. 3 (2013) 34–38.
[5] P. Sinsermsuksakul, K. Hartman, S.B. Kim, J. Heo, L. Sun, H.H. Park, R. Chakraborty, T. Buonassisi, R.G. Gordon, Appl. Phys. Lett. 102 (2013) 1–5 (053901).
[6] J.A. Bragagnolo, A.M. Barnett, J.E. Phillips, R.B. Hall, A. Rothwarf, J.D. Meakin, IEEE Trans. Electron Devices 27 (1980) 645–651.
[7] W. Septina, S. Ikeda, Y. Iga, T. Nakamura, T. Harada, M. Matsumura, Thin Solid Films 550 (2014) 700–704.
[8] Y. Nishi, T. Miyata, T. Minami, Thin Solid Films 528 (2013) 72–76.
[9] A. Kirkeminde, R. Scott, S. Ren, Nanoscale 4 (2012) 7649–7654.
[10] A.W. Welch, L.L. Baranowski, P. Zawadzki, C. DeHart, S. Johnston, S. Lany, C.A. Wolden, A. Zakutayev, Prog. Photovolt. Res. Appl. 24 (2016) 929–939.
[11] C. Yan, Z. Su, E. Gu, T. Cao, J. Yang, J. Liu, F. Liu, Y. Lai, J. Li, Y. Liu, RSC Adv. 2 (2012) 10481–10484.
[12] K. Ramasamy, H. Sims, W.H. Butler, A. Gupta, Chem. Mater. 26 (2014) 2891–2899.
[13] L. Wan, C. Ma, K. Hu, R. Zhou, X. Mao, S. Pan, L.H. Wong, J. Xu, J. Alloys Compd. 680 (2016) 182–190.
[14] L. Yu, R.S. Kokenyesi, D.A. Keszler, A. Zunger, Adv. Energy Mater. 3 (2013) 43–48.
[15] T. Rath, A.J. MacLachlan, M.D. Brown, S.A. Haque, J. Mater. Chem. A 3 (2015) 24155–24162.
[16] Y. Zou, J. Jiang, Mater. Lett. 123 (2014) 66–69.
[17] Mou Pal, N.R. Mathews, R. Silva Gonzalez, X. Mathew, Thin Solid Films 535 (2013) 78–82.
[18] A.C. Lokhande, K.V. Gurav, E. Jo, C.D. Lokhande, J.H. Kim, J. Alloys Compd. 656 (2016) 295–310.
[19] M.G. Panthani, V. Akhavan, B. Goodfellow, J.P. Schmidtke, L. Dunn, A. Dodabalapur, P.F. Barbara, B.A. Korgel, J. Am. Chem. Soc. 130 (2008) 16770–16777.
[20] M.V. Morales-Gallardo, A.M. Ayala, M. Pal, M.A. Cortes Jacome, J.A. Toledo Antonio, N.R. Mathews, Chem. Phys. Lett. 660 (2016) 93–98.
[21] C. Du, M. Xiao, Sci Rep 4 (2014) 1–5 (7339).
[22] J. Ning, K. Men, G. Xiao, L. Wang, Q. Dai, B. Zou, B. Liu, G. Zou, Nanoscale 2 (2010) 1699–1703.
[23] Q. Liang, K. Huang, X. Ren, W. Zhang, R. Xie, S. Feng, CrystEngComm 18 (2016) 3703–3710.
[24] S. Suehiro, K. Horita, M. Yuasa, T. Tanaka, K. Fujita, Y. Ishiwata, K. Shimanoe, T. Kida, Inorg. Chem. 54 (2015) 7840–7845.
[25] S. Ikeda, S. Sogawa, Y. Tokai, W. Septina, T. Harada, M. Matsumura, RSC Adv. 4 (2014) 40969–40972.
[26] D. Xu, S. Shen, Y. Zhang, H. Gu, Q. Wang, Inorg. Chem. 52 (2013) 12958–12962.
[27] C. An, Q. Liu, K. Tang, Q. Yang, X. Chen, J. Liu, Y. Qian, J. Cryst. Growth 256 (2003) 128–133.
[28] Mou Pal, N.R. Mathews, F. Paraguay-Delgado, X. Mathew, Mater. Chem. Phys. 166 (2015) 201–206.
[29] V. Vinayakumar, S. Shaji, D. Avellaneda, T.K. Das Roy, G.A. Castillo, J.A.A. Martinez, B. Krishnan, Sol. Energy Mater. Sol. Cells 164 (2017) 19–27.
[30] J. Baker, R.S. Kumar, D. Sneed, A. Connolly, Y. Zhang, N. Velisavljevic, J. Paladugu, M. Pravica, C. Chen, A. Cornelius, Y. Zhao, J. Alloys Compd. 643 (2015) 186–194.
[31] RRUFF Project Database, http://rruff.info/.
[32] S. Kar, S. Santra, H. Heinrich, J. Phys. Chem. C 112 (2008) 4036–4041.
[33] Z. Zhang, H. Zhang, Y. Fu, C. Zhou, Y. Lai, J. Electron. Mater. 44 (2015) 252–257.
[34] P. Dalvand, M.R. Mohammadi, J. Nanopart. Res. 13 (2011) 3011–3018.
[35] W. Qingqing, X. Gang, H. Gaorong, J. Solid State Chem. 178 (2005) 2680–2685.
[36] S. Dekhil, H. Dahman, S. Rabaoui, N. Yaacoub, L. El Mir, J. Mater. Sci. Mater. Electron. 28 (2017) 11631–11635.
[37] P. Kubelka, P.F. Munk, Z. Tech. Phys. 12 (1931) 593–601.